

1           **The effect of diffusion on asymmetric spin echo based quantitative BOLD:**

2           **An investigation of the origin of deoxygenated blood volume overestimation**

3           Alan J Stone<sup>1</sup>, Naomi C Holland<sup>2</sup>, Avery J L Berman<sup>3</sup>, Nicholas P Blockley<sup>1\*</sup>

4           <sup>1</sup>Wellcome Centre for Integrative Neuroimaging, FMRIB, Nuffield Department of Clinical

5           Neurosciences, University of Oxford, Oxford, UK, <sup>2</sup>Department of Physics, University of

6           Oxford, Oxford, UK, <sup>3</sup>Athinoula A. Martinos Center for Biomedical Imaging, Department of

7           Radiology, Harvard Medical School, Massachusetts General Hospital, Charlestown, MA

8

9           **Running Title:** The effect of diffusion on ASE qBOLD

10          **Address for correspondence:** \* Nicholas Blockley, School of Life Sciences, The University  
11          of Nottingham Medical School, Queen's Medical Centre, Nottingham, NG7 2UH, UK.

12          **Telephone No.:** +44 115 8230146

13          **E-mail:** nicholas.blockley@nottingham.ac.uk

14          **Twitter:** @nicblockley

15          **Word Count:** 5949

16          **Figures:** 8 figures and 1 table (+ 7 supplementary figures)

17          **References:** 33

18          **Funding Acknowledgements:** This work was supported by the Engineering and Physical

19          Sciences Research Council [grant number EP/K025716/1].

20

21

1 **Abstract**

2 Quantitative BOLD (qBOLD) is a technique for mapping oxygen extraction fraction (OEF)  
3 and deoxygenated blood volume (DBV) in the human brain. Recent measurements using an  
4 asymmetric spin echo (ASE) based qBOLD approach produced estimates of DBV which  
5 were systematically higher than measurements from other techniques. In this study, we  
6 investigate two hypotheses for the origin of this DBV overestimation and consider the  
7 implications for *in vivo* measurements. Investigations were performed by combining Monte  
8 Carlo simulations of extravascular signal with an analytical model of the intravascular signal.

9 *Hypothesis 1:* DBV overestimation is due to the presence of intravascular signal  
10 which is not accounted for in the analysis model. Intravascular signal was found to have a  
11 weak effect on qBOLD parameter estimates.

12 *Hypothesis 2:* DBV overestimation is due to the effects of diffusion which aren't  
13 accounted for in the analysis model. The effect of diffusion on the extravascular signal was  
14 found to result in a vessel radius dependent variation in qBOLD parameter estimates. In  
15 particular, DBV overestimation peaks for vessels with radii from 20 to 30  $\mu\text{m}$  and is OEF  
16 dependent. This results in the systematic underestimation of OEF.

17 *In vivo implications:* The impact on *in vivo* qBOLD measurements was investigated  
18 by simulating a distribution of vessel sizes with a small number of discrete radii.  
19 Overestimation of DBV consistent with previous experiments was observed, which was also  
20 found to be OEF dependent. This results in the progressive underestimation of the measured  
21 OEF. Furthermore, the relationship between the measured OEF and the true OEF was found  
22 to be dependent on echo time and spin echo displacement time.

23 The results of this study demonstrate the limitations of current ASE based qBOLD  
24 measurements and provides a foundation for the optimisation of future acquisition  
25 approaches.

## 1 **Introduction**

2 The quantitative BOLD (qBOLD) technique is a relaxometry based approach for mapping  
3 oxygen extraction fraction (OEF) and deoxygenated blood volume (DBV) in the human brain  
4 (He and Yablonskiy, 2007). An elevated OEF is indicative of tissue at risk of infarction, such  
5 as the penumbral tissue surrounding the core infarct of an ischaemic stroke (Astrup et al.,  
6 1981). When combined with a measurement of cerebral blood flow (CBF), the cerebral  
7 metabolic rate of oxygen consumption ( $CMRO_2$ ) can also be estimated (Kety and Schmidt,  
8 1948). Since qBOLD can provide this valuable information in a non-invasive and rapidly  
9 acquired manner, it has a great deal of potential for providing these quantitative physiological  
10 measurements in clinical research applications.

11 The analytical model used to analyse qBOLD data assumes that the signal decay  
12 behaves as though it were in the static dephasing regime (SDR) i.e. the diffusion of water in  
13 tissue does not influence the signal decay due to magnetic field inhomogeneity (Yablonskiy  
14 and Haacke, 1994). However, simulations of the Gradient Echo Sampling of Spin Echo  
15 (GESSE) pulse sequence, which is often used to acquire qBOLD data, have shown that this is  
16 not the case and that diffusion introduces a vessel size dependent effect on the signal decay  
17 (Dickson et al., 2010; Pannetier et al., 2014). However, qBOLD data can also be acquired  
18 using the Asymmetric Spin Echo (ASE) pulse sequence, and it is unclear whether a similar  
19 effect is observed in these experiments (An and Lin, 2003; Stone and Blockley, 2017).  
20 Interestingly estimates of DBV made using this ASE based acquisition are systematically  
21 higher than those reported for GESSE based measurements (He and Yablonskiy, 2007),  
22 suggesting that different effects may be at play.

23 The overestimation of DBV by ASE based qBOLD is at least partially responsible for  
24 the underestimation of the OEF (Stone and Blockley, 2017). This overestimation has  
25 previously been suggested to be due to the presence of intravascular blood signal, which is

1 not accounted for in the analytical qBOLD model, with flow crushing gradients proposed as a  
2 solution (An and Lin, 2003). However, since it has been shown that diffusion results in  
3 additional signal attenuation (Dickson et al., 2010), which is similarly unaccounted for in the  
4 analytical qBOLD model, this may also provide a mechanism for DBV overestimation.

5 In this study, we investigate both mechanisms to discover whether either can account  
6 for the overestimation of DBV in ASE based qBOLD. The effect of diffusion on the  
7 extravascular tissue signal was examined using Monte Carlo simulations (Boxerman et al.,  
8 1995a) and the intravascular blood signal was simulated using a recently published analytical  
9 model (Berman and Pike, 2018). Whilst these effects are initially considered using  
10 simulations with vessels of a single radius, these results are also integrated using an *in vivo*  
11 vessel size distribution to investigate sources of systematic error in real world measurements.

12

### 13 **Theory**

14 Transverse signal decay results from dephasing of the net magnetisation due to the presence  
15 of magnetic field inhomogeneity at multiple scales. The effect of these scales on the qBOLD  
16 signal can be considered with reference to a spin echo pulse sequence. At the microscopic  
17 scale spins experience local magnetic field inhomogeneities caused by neighbouring spins  
18 that are rapidly varying. Due to this rapid magnetic field variation, the phase evolution cannot  
19 be rewound by the application of a refocussing pulse. The resulting signal decay is described  
20 by the irreversible transverse relaxation rate  $R_2$ . The macroscopic scale describes magnetic  
21 field inhomogeneity on the scale of the head i.e. due to the nasal sinuses or ear canals. This  
22 effect can be reversed by a refocussing pulse due to its static nature, enabling the phase  
23 evolution in the period before the refocussing pulse to be rewound by the time the spin echo  
24 is formed. At this scale the signal decay is described by the reversible relaxation rate  $R_2'$  and  
25 referred to as the SDR. At intermediate scales, often referred to as the mesoscopic scale,

1 diffusion becomes increasingly important as the so called Diffusion Narrowing Regime is  
 2 approached. The transition between these regimes is dependent on the scale of the magnetic  
 3 field inhomogeneity and the distance the spin travels due to diffusion. More precisely, the  
 4 characteristic diffusion time ( $\tau_d \propto r^2/D$ ), which is dependent on the radius ( $r$ ) of the  
 5 deoxygenated blood vessel and the diffusion coefficient ( $D$ ), is on the order of the time taken  
 6 by a water molecule to diffuse a distance equivalent to the radius of the vessel (Yablonskiy  
 7 and Haacke, 1994). This results in an averaging of the magnetic field distribution surrounding  
 8 the vessels and a loss of phase history, meaning that signal cannot be efficiently recovered by  
 9 a refocussing pulse.

10

### 11 Modelling the qBOLD signal

12 The qBOLD model relies on the known relationship between  $R_2'$  and the baseline OEF,  $E_0$ ,  
 13 and deoxygenated blood volume,  $V_0$ , for a network of randomly oriented blood vessels  
 14 approximated as infinite cylinders (Yablonskiy and Haacke, 1994),

$$R_2' = \frac{4}{3} \pi \gamma B_0 \Delta\chi V_0 Hct E_0 \quad (1)$$

15 where  $\gamma$  is the proton gyromagnetic ratio,  $B_0$  is the main magnetic field,  $\Delta\chi$  is the difference  
 16 in volume magnetic susceptibility between fully oxygenated and fully deoxygenated blood  
 17 and  $Hct$  is the haematocrit. However, further modelling has shown that the  $R_2'$ -weighted  
 18 signal is not purely monoexponential, displaying a quadratic exponential behaviour around  
 19 the spin echo. Under the assumption that the signal decays in the SDR, the following solution  
 20 has been found,

$$S(\tau) = S_0 e^{-t_E R_2} e^{-V f_c(\tau R_2'/V)} \quad (2)$$

$$f_c(\tau R_2'/V) = \frac{1}{3} \int_0^1 du (2+u) \sqrt{1-u} \frac{1 - J_0(1.5 \tau (R_2'/V) u)}{u^2} \quad (3)$$

1 where  $t_E$  is the echo time,  $\tau$  is the spin echo displacement time and  $J_0$  is the zeroth-order  
 2 Bessel function (He and Yablonskiy, 2007). For simplicity this continuous function can be  
 3 broken down into two asymptotic solutions and applied piece wise (An and Lin, 2000).

$$S^S(\tau) = S_0 e^{-t_E R_2} e^{-0.3 (\tau R_2')^2 / V}, \quad \tau < \frac{1.5 V}{R_2'} \quad (4)$$

$$S^L(\tau) = S_0 e^{-t_E R_2} e^{-\tau R_2' e^V}, \quad \tau > \frac{1.5 V}{R_2'} \quad (5)$$

4 In the long  $\tau$  regime (Eq. (5)) the signal decay takes a monoexponential form, whilst in the  
 5 short  $\tau$  regime (Eq. (2)) the signal follows a quadratic exponential form. A log-linear fit to  
 6 long  $\tau$  data enables  $R_2'$  to be estimated. Furthermore, comparison of the measured signal at  
 7  $\tau=0$  ( $S_{meas}^S(0)$ ) with the intercept extrapolated from long  $\tau$  data ( $S_{extrap}^L(0)$ ) enables  $V_0$  to be  
 8 calculated.

$$V_0 = \ln S_{extrap}^L(0) - \ln S_{meas}^S(0) \quad (6)$$

9 Henceforth we will refer to this as the SDR qBOLD model.

10

### 11 Simulating the effect of diffusion

12 Monte Carlo simulations of the qBOLD signal were performed by repeating the following  
 13 three steps for each simulated proton.

14 Step 1: Generate a system of vessels. The vessel system was defined as a sphere with  
 15 radius  $R_s$ . Vessel origin points ( $O$ ) were randomly selected, with half placed on the surface of  
 16 the sphere and half within the sphere (Dickson et al., 2010). A uniform distribution of points  
 17 over the surface of the sphere was ensured by generating a unit vector ( $X_i$ ) from a normally  
 18 distributed random number generator (mean 0, standard deviation 1) and scaling by  $R_s$   
 19 (Muller, 1959). Within the sphere, uniform density was maintained by taking account of the  
 20 increased volume occupied by points far from the centre of the system. This scaling factor,  $U$ ,  
 21 is selected from a uniform distribution of random numbers (range 0 to 1).

$$(O_1, O_2, O_3) = \begin{cases} R_s \frac{(X_1, X_2, X_3)}{\sqrt{X_1^2 + X_2^2 + X_3^2}}, & \text{on sphere surface} \\ R_s U \frac{(X_1, X_2, X_3)}{\sqrt{X_1^2 + X_2^2 + X_3^2}}, & \text{within sphere} \end{cases} \quad (7)$$

1 Vessels are modelled as randomly oriented infinitely long cylinders with a single radius,  $R_c$ ,  
 2 placed at the vessel origin points described by Eq. (7) and added until the target volume  
 3 fraction ( $V_f$ ) is reached. Random orientation was ensured by generating a unit vector from a  
 4 normally distributed random number generator (mean 0, standard deviation 1).

5 Step 2: Proton random walk. Protons are initially placed at the centre of the vessel  
 6 system. Each step taken by the proton is independently selected along each dimension from a  
 7 normal distribution of random numbers with mean 0 and standard deviation  $\sigma$  with diffusion  
 8 coefficient,  $D$ , and time interval between steps,  $\Delta t$ .

$$\sigma = \sqrt{2 D \Delta t} \quad (8)$$

9 Step 3: Estimate the phase accrued at each step. The phase,  $\Delta\phi$ , accumulated by the  
 10 proton during each time interval is calculated by summing over the field contributions from  
 11 all  $N$  vessels (Boxerman et al., 1995a),

$$\Delta\phi = 2\pi \gamma B_0 \Delta t (1 - Y) Hct \Delta\chi \sum_{i=1}^N \left(\frac{R_c}{r_i}\right)^2 \cos 2\varphi_i \sin^2 \theta_i, \quad r \geq R \quad (9)$$

12 where  $\theta$  is the angle of the vessel with respect to  $B_0$ ,  $\varphi$  is the angle with respect to the  
 13 projection of  $B_0$  onto a plane orthogonal to the vessel,  $r_i$  is the perpendicular distance to the  
 14 vessel and  $Y$  is the blood oxygen saturation. Only the equation for the magnetic field outside  
 15 of the vessel is presented, since only extravascular signal was simulated.

16 By appropriate combination of the phase accrued in each interval it is possible to  
 17 simulate the phase evolution of the ASE and GESSE pulse sequences as a function of  $\tau$ ,  
 18  $\phi(\tau)$ .

$$\phi(\tau) = \sum_{j=1}^m \Delta\phi_j - \sum_{j=m+1}^n \Delta\phi_j \quad (10)$$

1 where  $m$  defines the transition from signal decay to signal recovery due to the refocussing  
 2 pulse,  $n$  is the point at which the signal is acquired and where  $0 \leq m \leq n$ . For ASE  $m =$   
 3  $(t_E - \tau) / 2 \Delta t$  and  $n = t_E / \Delta t$ , whilst for GESSE  $m = t_{SE} / 2 \Delta t$  and  $n = (t_{SE} + \tau) / \Delta t$ .  
 4 Here,  $t_E$  is defined as the timing of the centre of the readout and  $t_{SE}$  is the time at which the  
 5 spin echo forms (see Fig. 1). These definitions reflect an important distinction between the  
 6 ASE and GESSE pulse sequences, whereby  $t_E$  is fixed for ASE and variable for GESSE  
 7 whilst  $t_{SE}$  is variable for ASE and fixed for GESSE.

8 The phase evolution of  $P$  protons is then summed to simulate the decay of the  
 9 extravascular ASE or GESSE signal (Boxerman et al., 1995a),

$$S_{EV}(t_E, \tau) = \left| \frac{1}{P} \sum_{k=1}^P e^{i\phi(\tau)} \right| e^{-\frac{t_E}{T_{2,t}}} \quad (11)$$

10

11 where  $T_{2,t}$  is the underlying tissue  $T_2$ .

12 Intravascular signal has traditionally been difficult to simulate, with empirical  
 13 measurements of blood  $R_2$  and  $R_2^*$  commonly used (Griffeth and Buxton, 2011). However,  
 14 simulating the  $R_2'$ -weighted signal using the difference between  $R_2$  and  $R_2^*$  is likely to be  
 15 inaccurate in the short  $\tau$  regime. Recently an analytical model of the blood signal during a  
 16 Carr-Purcell Meiboom-Gill (CPMG) pulse sequence was extended to capture the signal  
 17 evolution between an arbitrary number of spin echoes (Berman and Pike, 2018), i.e. the  
 18 conditions that exist for ASE and GESSE pulse sequences. Using this model, the  
 19 intravascular signal,  $S_{IV}$ , is described by,

$$S_{IV}(t_E, \tau) = \exp \left\{ -\frac{\gamma^2}{2} G_0 \tau_D^2 \left[ \frac{t_E}{\tau_D} + \left( \frac{1}{4} + \frac{t_E}{\tau_D} \right)^{\frac{1}{2}} + \frac{3}{2} - 2 \left( \frac{1}{4} + \frac{t_E - t_{SE}/2}{\tau_D} \right)^{\frac{1}{2}} \right] \right\} \quad (12)$$



$$2 \left( \frac{1}{4} + \frac{t_{SE}/2}{\tau_D} \right)^{\frac{1}{2}} \exp \left( -\frac{t_E}{T_{2,b|0}} \right).$$

- 1 Here  $\tau_D = R_{\text{rbc}}^2/D_b$ , where  $R_{\text{rbc}}$  is the characteristic size of red blood cells and  $D_b$  is the  
 2 diffusion coefficient of blood,  $T_{2,b|0}$  is the intrinsic  $T_2$  of blood and  $G_0$  is the mean square field  
 3 inhomogeneity in blood,

$$G_0 = \frac{4}{45} Hct (1 - Hct) (4 \pi \Delta \chi (0.95 - Y) B_0)^2. \quad (13)$$

- 4 The value of  $t_{SE}$  is fixed for GESSE but is variable for ASE with  $t_{SE} = t_E - \tau$ . By definition  
 5  $t_E$  is fixed for ASE and varying for GESSE.

- 6 Finally, the total signal,  $S_{TOT}$ , is calculated by taking a volume weighted sum of the  
 7 intra- and extravascular signals.

$$S_{TOT} = (1 - V_f) S_{EV} + V_f S_{IV} \quad (14)$$

8

## 9 **Methods**

10

### 11 Simulations

- 12 Simulations of the tissue signal were performed following the theory outlined above. Firstly,  
 13 extravascular signal decay was simulated using Monte Carlo simulations ( $B_0=3$  T,  
 14  $\gamma=267.5 \times 10^6$  rad s<sup>-1</sup> T<sup>-1</sup>). The radius of the spherical system of vessels,  $U$ , was chosen to  
 15 maintain a similar number of vessels,  $N$ , regardless of the vessel radius ( $N \sim 1,300$ ). For each  
 16 proton, a complete random walk was generated with a step size,  $\Delta t$ , of 20  $\mu$ s, which was  
 17 downsampled to 200  $\mu$ s, and  $D=1$   $\mu\text{m}^2\text{ms}^{-1}$ . The perpendicular distance,  $r_i$ , to each vessel in  
 18 the system was then calculated. For protons that passed close to vessels, defined as  $R_c^2/r_i^2 >$   
 19 0.04, the perpendicular distance was recalculated using the original 20  $\mu$ s time step to better  
 20 sample the rapid magnetic field variation expected close to vessels (Dickson et al., 2010).  
 21 Walks that moved the proton inside a vessel were flagged to be discarded in order to simulate

1 non-permeable blood vessels. The phase of each proton was allowed to evolve for 120 ms  
2 after the excitation with  $\Delta\chi=0.27$  ppm (Spees et al., 2001). Phase accrual was stored for each  
3 proton in 2 ms intervals,  $\Delta t$ . A new system of vessels was generated for each proton and a  
4 total of 10,000 protons were simulated for each vessel radius investigated. However, the  
5 number of protons that passed within a vessel increased rapidly for smaller vessel radii.  
6 Therefore, only the first  $P=5,000$  protons that did not pass within a vessel were used to  
7 calculate  $S_{EV}$  using Eq. (11) with  $T_{2,t}=80$  ms. Secondly, intravascular signal decay was  
8 simulated using Eqs. (12) and (13), which are independent of vessel radius. Based on  
9 previous work the following parameters were used (Berman et al., 2017):  $T_{2,b0}=189$  ms,  
10  $R_{rbc}=2.6$   $\mu\text{m}$  and  $D_b=2$   $\mu\text{m}^2\text{ms}^{-1}$ . The total signal was then calculated using Eq. (14).

11 Whilst the intravascular simulations are rapid to perform, Monte Carlo simulations of  
12 the extravascular signal are time consuming. Therefore, the following approaches were taken  
13 to accelerate these simulations, with examples presented as supplementary figures. We have  
14 previously shown that different oxygenation levels can be simulated by scaling the accrued  
15 phase of a nominal oxygenation value by the target value (Blockley et al., 2008). This is  
16 made possible by saving the phase of each proton and the fact that phase is a linear function  
17 of blood oxygenation for a network of vessels with the same oxygenation (Fig. S1). Different  
18 volume fractions can be simulated from the signal magnitude generated by Eq. (11). It has  
19 been shown that the extravascular signal,  $S_{EV}$ , can be described as a radius dependent shape  
20 function,  $f(R_c, \tau)$ , scaled by the volume fraction (Dickson et al., 2011; Kiselev and Posse,  
21 1999) (Fig. S2).

$$S_{EV}(R_c, \tau) = \exp[-V_f(R_c)f(R_c, \tau)] \quad (15)$$

22 Finally, it is possible to simulate the effect of a system with multiple vessel radii by  
23 combining multiple single vessel radius simulations of the extravascular signal (Dickson et  
24 al., 2011; Kiselev and Posse, 1999). The resulting combined signal,  $S_{EV}^{MULTI}$ , can be calculated

1 as the product of the signals of  $M$  single vessel simulations which have already been scaled  
 2 for blood oxygenation and volume fraction as described above (Fig. S3).

$$S_{EV}^{MULTI} = \prod_{k=1}^M S_{EV}(k) \quad (16)$$

3

#### 4 Parameter quantification

5 The following framework was used to quantify the parameters of the qBOLD model from the  
 6 simulated decay curves. The parameters of the SDR qBOLD model ( $R_2'$  and DBV) were  
 7 organised as a vector of unknowns ( $x$ ) in a linear system ( $A \cdot x = B$ ) (Stone et al., 2019). The  
 8 first row of the matrix  $A$  represents Eq. (4) when  $\tau=0$  with subsequent rows representing Eq.  
 9 (5) with values of  $\tau$  beyond the transition between the quadratic and linear exponential  
 10 regime. In this case only values of  $\tau$  greater than 15 ms were used. Vector  $B$  contains the  
 11 ASE signals,  $S(\tau)$ .

$$\begin{bmatrix} 0 & 0 & 1 \\ 1 & -\tau_1 & 1 \\ 1 & -\tau_2 & 1 \\ \vdots & \vdots & \vdots \\ 1 & -\tau_n & 1 \end{bmatrix} \begin{bmatrix} V_0 \\ R_2' \\ \log(S_0) - t_E \cdot R_2' \end{bmatrix} = \begin{bmatrix} \log(S(0)) \\ \log(S(\tau_1)) \\ \log(S(\tau_2)) \\ \vdots \\ \log(S(\tau_n)) \end{bmatrix} \quad (17)$$

12 Parameters were estimated via Eq. (17) using the least square solution, with the error in each  
 13 parameter determined from the covariance matrix. Finally, OEF can be estimated by  
 14 rearranging Eq. (1).

$$E_0 = \frac{3 \cdot R_2'}{4\pi \cdot \gamma B_0 \cdot \Delta\chi_0 \cdot Hct \cdot V_0} \quad (18)$$

15

#### 16 Effect of diffusion on ASE measurements

17 Initial simulations were performed for a selection of vessel radii ( $R_c=5, 10, 50, 1000 \mu\text{m}$ ), a  
 18 venous  $Y$  of 60%, a Hct of 40% and a DBV of 3%. Simulations of the ASE pulse sequence  
 19 were performed with  $t_E=60$  ms and  $-60 \text{ ms} \leq \tau \leq 60$  ms for both extra- and intravascular

1 signal, where  $\tau=60$  ms corresponds to pure gradient echo decay. For validation purposes,  
2 similar simulations were performed for the GESSE pulse sequence using  $t_{SE}=60$  ms and -30  
3 ms  $\leq \tau \leq 60$  ms.

4

#### 5 Effect of diffusion on qBOLD parameters

6 A further set of synthetic ASE signal decay curves were generated for vessel radii  
7 logarithmically spaced between 1 and 1,000  $\mu\text{m}$ . All other parameters were set consistent  
8 with previous qBOLD measurements (Stone and Blockley, 2017). In the context of these  
9 simulations this required  $t_E=80$  ms with  $\tau=0$  and  $\tau=16$  to 64 ms in 4 ms steps. The *apparent*  
10 value of  $R_2'$ , DBV and OEF were then estimated using Eq. (17) and (18). The effect of  
11 diffusion on the estimation of qBOLD parameters was investigated by first fixing OEF and  
12 varying DBV and then by fixing DBV and varying OEF. In the former case a fixed OEF of  
13 40% was coupled with DBV values of 1, 3 and 5%, whilst in the latter case DBV was fixed at  
14 3% and OEF took values of 20, 40 and 60%. These values are considered to be the *true*  
15 parameters in both cases. The results of varying DBV were also used to consider the  
16 percentage error in DBV as a function of vessel radius. In these single vessel simulations  
17 arterial blood is assumed to have an oxygen saturation,  $Y$ , of 100% hence the venous  
18 saturation,  $Y_v = 1 - E_0$ .

19 The effect of intravascular signal on qBOLD parameter estimates was investigated by  
20 repeating these simulations, but excluding the intravascular compartment. In this way it was  
21 possible to quantify the percentage of the parameter estimate (PE) which results from the  
22 presence of intravascular signal i.e.  $(PE_{EV} - PE_{EV+IV})/PE_{EV+IV}$ .

23 Further investigation of the effect of diffusion on DBV estimates was pursued based  
24 on a consideration of Eq. (6), which suggests that errors must be due to either the signal  
25 measured at  $\tau=0$  ( $S_{meas}^S(0)$ ) or the extrapolated estimate of the signal at  $\tau=0$  from the  $R_2'$  fit

1 ( $S_{extrap}^L(0)$ ), or both. However, given the analysis approached represented by Eq. (17)  
2  $S_{extrap}^L(0)$  is not estimated and  $S_{meas}^S(0)$  is confounded by  $T_2$  decay. The latter was corrected  
3 by calculating the signal decay relative to the value at  $R=1,000 \mu\text{m}$ , where previous  
4 simulations would suggest the SDR applies and hence signal attenuation should be zero. The  
5 former was estimated by subtracting this relative measure of  $S_{meas}^S(0)$  from the estimated  
6 value of apparent DBV.

7

### 8 Effect of an *in vivo* vessel radius distribution

9 The *in vivo* effect of a distribution of vessel radii was investigated by integrating the results  
10 from single radius simulations. A compartmental model of the vasculature derived from the  
11 morphology of the sheep brain was selected (Sharan et al., 1989). This model has five orders  
12 of arterial and venous vessels, with a range of radii, and a capillary compartment with a  
13 single vessel radius (Table 1). Additional Monte Carlo simulations for this range of vessel  
14 radii were performed and combined using the acceleration techniques described above.  
15 Arterial vessels were assigned an arterial oxygen saturation,  $Y_a$ , of 98%, which was used to  
16 calculate the venous saturation,  $Y_v$ , for a given OEF.

$$Y_v = Y_a(1 - E_0) \quad (19)$$

17 The capillary compartment was an intermediate oxygen saturation,  $Y_c$ , calculated as an  
18 average of the arterial and venous saturations weighted by a factor,  $\kappa$ , equal to 0.4  
19 representing a weighting towards the venous saturation (Griffeth and Buxton, 2011; Tsai et  
20 al., 2003).

$$Y_c = \kappa Y_a + (1 - \kappa) Y_v \quad (20)$$

21 Relative blood volume fractions for each vessel type were calculated by estimating the  
22 volume of each vessel radius population as cylinders with the properties described in Table 1.  
23 These relative blood volume fractions were then scaled by the total cerebral blood volume

1 (CBV). Pairs of OEF and CBV values were drawn from a uniform random number generator  
2 within the following ranges: OEF 0-100%, CBV 0-10%. The qBOLD parameters were  
3 quantified for 1,000 random OEF-CBV pairs to examine the effect of diffusion across the  
4 physiological range. In the absence of a strict definition of DBV, the ground truth was  
5 assumed to be equal to the combined blood volume occupied by capillary and venous vessels.  
6 This is therefore only a working assumption, since it is likely the *true* DBV is weighted by  
7 blood oxygenation and vessel radius. Deoxyhaemoglobin content, dHb, was calculated based  
8 on the same assumption for DBV and a value for the density of brain tissue  $\rho=1.04$  g/ml  
9 (Rempp et al., 1994) using the following equation.

$$dHb = 100 \frac{V_0}{\rho} \frac{Hct}{0.03} E_0 \quad (21)$$

10 For comparison these simulations were also repeated for the original ASE based qBOLD  
11 implementation with  $t_E=64$  ms with  $\tau=0$  and  $\tau=10$  to 18 ms in 4 ms steps (An and Lin, 2003).

12 Details on how to access the simulation code, simulation results and analysis code  
13 that underlie this study can be found in Appendix A.

14

## 15 **Results**

16 Figure 2 presents simulations of the signal generated by the ASE pulse sequence in the  
17 absence of  $T_2$  decay. The extravascular signal (Fig. 2a) was found to be symmetric with  
18 respect to the spin echo ( $\tau=0$ ) regardless of vessel radius. Similarly, the intravascular signal  
19 (Fig. 2b) was symmetric, but displayed a relatively weak signal decay as a function of  $\tau$ . In  
20 contrast, simulations of the GESSE pulse sequence demonstrated increasing asymmetry with  
21 reducing vessel radius for the extravascular signal and strong asymmetry for the intravascular  
22 signal (Fig. S4).

23 Figure 3 displays the effect of vessel size on the parameter estimates from the SDR  
24 qBOLD model. The apparent values of  $R_2'$  plateau above a critical vessel radius of

1 approximately 40  $\mu\text{m}$  (Fig. 3a,d) and are then consistent with predictions from the SDR  
2 qBOLD model (dashed lines calculated using Eq. (1)). The apparent DBV is found to be  
3 strongly dependent on vessel radius, peaking between 20 and 30  $\mu\text{m}$  (Fig. 3b,e). Estimates of  
4 the apparent OEF increase monotonically with vessel radius reaching the value predicted by  
5 the SDR qBOLD model as the vessel radius approaches 1,000  $\mu\text{m}$  (Fig. 3c,f). When the true  
6 OEF was fixed whilst DBV was varied (Fig. 3c) estimates of apparent OEF were consistent  
7 across DBV levels, suggesting that the error in DBV is a linear scale factor. Likewise, it can  
8 be seen that the profile of apparent DBV when the true DBV was fixed and OEF was varied  
9 (Fig. 3e) peak at different vessel radius values, suggesting that the error in DBV is OEF  
10 dependent. Furthermore, this effect can be seen to result in a reduced dynamic range for the  
11 estimates of apparent OEF as vessel size is reduced (Fig. 3f). Figure 4 confirms that the  
12 percentage error in DBV is constant for a given combination of OEF and vessel radius (Fig.  
13 4a), but differs for different OEF values (Fig. 4b).

14 Figure 5 considers the contribution of intravascular signal to the parameter estimates  
15 in Fig. 3 as a function of vessel radius. This contribution is generally small for  $R_2'$  and DBV  
16 at around  $\pm 1\%$  for vessel radii greater than 10  $\mu\text{m}$ . However, the intravascular signal appears  
17 to reflect a larger contribution when OEF is low, conditions where qBOLD contrast is low.  
18 Despite this the effect of the intravascular signal appears to be largely cancelled in the  
19 estimation of OEF (Fig. 5c,f). A reproduction of Fig. 3 without intravascular signal is  
20 included in the supplementary material for comparison and shows little discernible difference  
21 by eye (Fig. S5).

22 Figure 6 investigates the origin of the DBV estimation error attributed either to an  
23 error in the measured signal at  $\tau=0$  (orange markers) or an error in the intercept extrapolated  
24 from long  $\tau$  data (green markers). In the case of the former,  $-\ln S_{meas}^S(0)$  is plotted such that  
25 the sum of the two curves representing the apparent DBV (represented by grey shading).

1 When interpreting these curves, it is useful to consider the orange markers as a reflection of  
2 the deviation of the spin echo from perfect refocusing (with positive values representing  
3 increased signal attenuation) and the green markers as a reflection of the deviation of the  
4 measured  $R_2'$  from the SDR qBOLD estimate of  $R_2'$ . The former is found to be subject to  
5 increasing signal attenuation as vessel size is reduced, which is strongly affected by blood  
6 oxygenation via OEF. The latter is found to plateau and is relatively consistent with the SDR  
7 qBOLD model for vessel radii greater than approximately 20  $\mu\text{m}$ .

8 Figure 7 explores the combined effect of a distribution of vessel radii on parameter  
9 estimates from the SDR qBOLD model. The apparent  $R_2'$  is plotted against values of  $R_2'$   
10 predicted by the SDR model via Eq. (1), with DBV estimated according to the working  
11 assumption described above (Fig. 7a). Data points are colour coded to reflect the true voxel  
12 deoxyhaemoglobin content in  $\text{ml}^{\text{dHb}}/100 \text{ g}^{\text{tissue}}$ . A linear dependence is maintained, albeit with  
13 a shallower gradient than predicted by the SDR qBOLD model. A large amount of  
14 uncertainty is observed in estimates of apparent DBV over the large physiological range  
15 tested (Fig. 7b), with data points colour coded by true OEF value. However, this level of  
16 uncertainty does not propagate into estimates of apparent OEF (Fig 7c) where data points are  
17 colour coded by true DBV. Apparent OEF increases monotonically between 0 and 50%, but  
18 reaches a plateau for higher values, and is inappropriately scaled compared with the true  
19 OEF. In a similar manner to Fig. 4, the percentage error in the apparent DBV can be plotted  
20 as a function of true OEF (Fig. 8). As noted for the single vessel radius simulations, this error  
21 is strongly OEF dependent.

22 These simulations were repeated for different ASE pulse sequence parameters,  
23 namely variations in  $t_E$  and  $\tau$ , and included in supplemental material. The results in Fig. S6  
24 largely mirror those in Fig. 7 with the following variations. The slope of the relationship  
25 between apparent  $R_2'$  and SDR qBOLD predicted  $R_2'$  is slightly reduced for the alternative



1 parameters (Fig. S6a). More noticeable is the reduction in the range of apparent DBV values  
2 (Fig. S6b), with the error in the apparent DBV reduced by more than a half (Fig. S7). Whilst  
3 the apparent OEF is also inappropriately scaled, the relationship with true OEF is more  
4 monotonic in nature.

5

## 6 **Discussion**

7 In this study numerical simulations were used to investigate the effect of diffusion on ASE  
8 based qBOLD measurements and the origin of DBV overestimation in such measurements. In  
9 contrast to the previously observed shift of the GESSE signal maximum due to the effect of  
10 diffusion, the ASE signal was observed to maintain its symmetry as vessel radius is reduced  
11 and the effect of diffusion is increased. Two hypotheses for the origin of the observed DBV  
12 overestimation were tested: (i) the effect of intravascular blood signal and (ii) the effect of  
13 diffusion on the extravascular tissue signal. The presence of intravascular blood signal was  
14 found to have a minor effect on qBOLD parameter estimates. It is therefore unlikely to be  
15 responsible for the majority of the overestimation observed in DBV measurements. In  
16 contrast, the extravascular signal was shown to have a very strong dependence on vessel  
17 radius providing the potential for a large error in DBV and is considered to be the dominant  
18 cause of DBV overestimation. Furthermore, the error in DBV is predicted to be blood oxygen  
19 saturation level dependent. Integration of these single vessel radius simulations via an *in vivo*  
20 vessel distribution revealed three main findings. Firstly, that the relationship between the  
21 apparent  $R_2'$  and deoxyhaemoglobin content is retained. Secondly, there is an inherent  
22 uncertainty in estimates of DBV. Finally, this uncertainty is not propagated to apparent OEF  
23 estimates, but results in inappropriate scaling of these estimates. Furthermore, the monotonic  
24 behaviour of the relationship between apparent and true OEF was found to be dependent on  
25 the pulse sequence parameters  $t_E$  and  $\tau$ . These results provide new directions for improving

1 the modelling of ASE qBOLD signal and the reduction of systematic error in parameter  
2 estimates of OEF and DBV.

3

#### 4 Effect of diffusion on ASE measurements

5 Whilst several studies have investigated the qBOLD signal as acquired by the GESSE pulse  
6 sequence (Christen et al., 2014; Dickson et al., 2011, 2010; Pannetier et al., 2014), this study  
7 considered whether the signal decay under an ASE acquisition behaves in the same way. One  
8 particular characteristic of the GESSE pulse sequence concerns the maximum of the qBOLD  
9 signal decay curve. This would ordinarily be expected to coincide with the spin echo ( $\tau=0$ ),  
10 but has been shown to be shifted towards negative  $\tau$  values (Fig. S4a) for the GESSE  
11 sequence in the presence of diffusion (Dickson et al., 2010; Pannetier et al., 2014). However,  
12 this effect is not observed in simulations of the extravascular signal acquired using an ASE  
13 pulse sequence (Fig. 2a), where the signal maximum was found to be close to the spin echo  
14 ( $\tau=0$ ). However, the GESSE and ASE sequences differ in an important way. The  $t_E$  of each  
15 successive  $\tau$  value increases in the GESSE experiment and hence the time for protons to  
16 diffuse around blood vessels increases. Whilst the  $t_E$  is constant for all  $\tau$  values in the ASE  
17 method and hence the time for diffusion is also constant. This would suggest that there is a  $t_E$   
18 dependent component of the  $R_2'$ -weighted signal decay. Such a component has previously  
19 been included as a correction to estimates of  $R_2'$  (Berman et al., 2017).

20 This study also considered the  $R_2'$ -weighted contribution of the blood to the qBOLD  
21 signal using a recently proposed model (Berman and Pike, 2018). In common with the  
22 extravascular results, the ASE blood signal is symmetric with respect to the spin echo, but  
23 decays far less as a function of  $\tau$  (Fig. 2b). However, the signal is heavily attenuated at all  $\tau$   
24 values compared with the extravascular simulations. This is in contrast to simulations of the

1 GESSE blood signal, which are highly shifted to negative  $\tau$  values and present largely as an  
2 exponential decay (Fig. S4b).

3

#### 4 Origin of DBV overestimation

5 Simulations of the combined intravascular and extravascular signal revealed a vessel radius  
6 dependent overestimation of DBV (Fig. 3b,e). The error in the apparent DBV was found to  
7 be OEF dependent (Fig. 4). However, at larger radii (approaching 1 mm) estimates of DBV  
8 were consistent with ground truth values. The contribution of intravascular signal to these  
9 parameter estimates was performed by comparing simulations with (Fig. 3) and without (Fig.  
10 S5) an intravascular compartment. A small and largely vessel radius independent effect (for  
11  $R_c > 10 \mu\text{m}$ ) was observed (Fig. 5b,e). The effect of intravascular signal was more pronounced  
12 for smaller vessel radii and low OEF, where the relative contribution of intravascular signal is  
13 increased by weak extravascular contrast. Despite this, the overestimation of DBV is  
14 dominated by the effect of diffusion on the extravascular signal.

15 Finally, Eq. (6) provides the opportunity to consider whether the systematic error in  
16 DBV originates in the measurement of the spin echo ( $S_{meas}^S(0)$ ), the intercept extrapolated  
17 from the long  $\tau$  regime ( $S_{extrap}^L(0)$ ) or a combination of both, as explored in Fig. 6. For  
18 vessel radii greater than  $20 \mu\text{m}$  additional signal attenuation of  $S_{meas}^S(0)$  is the main driver of  
19 overestimation of DBV. However, for vessels with radii below  $20 \mu\text{m}$ , errors in  $S_{extrap}^L(0)$   
20 provide an additional confound to DBV estimation. These results are consistent with the  
21 characteristics of gradient echo versus spin echo BOLD vessel size sensitivity, which  
22 correspond to  $\ln S_{extrap}^L(0)$  and  $\ln S_{meas}^S(0)$ , respectively (Boxerman et al., 1995b). For the  
23 smallest vessel radii the apparent  $R_2'$  is reduced relative to the value expected by the SDR  
24 qBOLD model (Fig. 3a,d) due to diffusional narrowing, such that  $\ln S_{extrap}^L(0)$  is also  
25 reduced (Fig. 6). Similarly, additional unrecoverable signal decay due to diffusion narrowing

1 results in a decrease in the value of  $\ln S_{meas}^S(0)$ , which is analogous to an increase in  
2 apparent  $R_2'$  and is strongest for capillary sized vessels (Note that Fig. 6 plots  
3  $-\ln S_{meas}^S(0)$ ). With increasing vessel radius,  $R_2'$  approaches the SDR qBOLD model  
4 prediction and the value of  $\ln S_{extrap}^L(0)$  approaches a constant value. Similarly the  
5 attenuation of the spin echo is reduced as the SDR is approached and  $\ln S_{meas}^S(0)$  reaches its  
6 minimum. Therefore, when the differing profiles of these phenomena are combined the form  
7 of the apparent DBV as a function of vessel radius can be described.

8

### 9 Effect of an *in vivo* vessel radius distribution

10 Having established the vessel radius dependence of the qBOLD signal, the implications for  
11 the *in vivo* condition were considered. In order to integrate the single vessel radius results, a  
12 vessel distribution with a small number of discrete vessel radii was selected. This enabled  
13 different oxygenation levels to be associated with different vessel types. A wide  
14 physiological range was investigated by randomly selecting pairs of OEF and CBV values.  
15 The apparent  $R_2'$  was found to be tightly correlated with the  $R_2'$  predicted by SDR qBOLD  
16 model (Fig. 7a). This is important as it demonstrates that the relationship between  $R_2'$  and the  
17 voxel deoxyhaemoglobin content (proportional to the product of deoxyhaemoglobin  
18 concentration and DBV) is maintained despite the effects of diffusion. It should therefore be  
19 possible to quantify maps of  $R_2'$  in terms of deoxyhaemoglobin content with appropriate  
20 scaling. Likewise with improved quantification of DBV, either through improvements to the  
21 qBOLD technique or via an additional experimental technique (Blockley et al., 2013; Lee et  
22 al., 2018), accurate measurements of OEF are possible. A large amount of uncertainty was  
23 observed in the apparent DBV (Fig. 7b). This was demonstrated to be blood oxygenation  
24 dependent i.e. a function of OEF (Fig. 8). This is consistent with the results of the single  
25 vessel simulations (Fig. 4) and demonstrates the important contribution of smaller vessel

1 radii. This also explains why this uncertainty does not propagate into the apparent OEF, since  
2 the percentage error in apparent DBV is constant at each OEF level (Fig. 7c). However, the  
3 increasing percentage error in apparent DBV with OEF (Fig. 8) results in a progressive  
4 underestimation of apparent OEF. A plateau in the apparent OEF limits the maximum  
5 measured OEF to approximately 50%. Despite this the remaining range covers the majority  
6 of the expected healthy physiological range (Marchal et al., 1992). These simulation were  
7 repeated for an alternative set of ASE pulse sequence parameters, replicating the effects  
8 observed for  $R_2'$  and DBV (Fig S6a,b and Fig. S7). However, a monotonic relationship  
9 between apparent and true DBV was revealed suggesting that a shorter  $t_E$  and/or maximum  $\tau$   
10 value could enable the technique to be sensitive to a broader range of OEF values.

11 Finally, the results of these multi-radius simulations appear to be consistent with  
12 previous measurements of  $OEF=21\pm 2\%$  and  $DBV=3.6\pm 0.4\%$  (Stone and Blockley, 2017).  
13 Under the assumption that a true OEF of 40% is healthy, Fig. 7 would predict an apparent  
14 OEF of 23%. Likewise Fig. 8 would predict the percentage error in the apparent DBV is  
15 100%, which would reduce the measured value above to 1.8%. This would bring these  
16 measurements in line with other MR based measurements of DBV at 1.75% (He and  
17 Yablonskiy, 2007) and venous CBV at 2.2% (Blockley et al., 2013).

18

### 19 Future work and Limitations

20 Whilst the simulation methodology used in this study has identified some limitations of the  
21 current implementation of ASE based qBOLD, it also offers an opportunity to optimise future  
22 implementations. Further simulations could be used to identify optimal values of  $t_E$  and  $\tau$   
23 which maximise the linearity of the relationship between apparent OEF and the ground truth.  
24 They could also be used to estimate a more appropriate scale factor for OEF estimation by

1 treating the  $\frac{4}{3}\pi$  geometry factor in Eq. (1) as an arbitrary scale factor. Such an approach has  
2 previously been used in calibrated BOLD to great effect (Griffeth and Buxton, 2011).

3 The results of this study rely on a detailed model of the qBOLD signal. However, in  
4 this implementation it only accounts for the intra- and extravascular signal contributions of a  
5 single distribution of blood vessels in grey matter. Whilst this two compartment model was  
6 sufficient to investigate the origin of DBV overestimation in ASE based qBOLD, a more  
7 realistic model might include the signal contributions of cerebral spinal fluid (Dickson et al.,  
8 2009), the myelin in white matter (Bouvier et al., 2013), desaturated arterial blood vessels  
9 (Boas et al., 2008), the effect of iron deposition (Wisner et al., 1988) or different vessel  
10 radius distributions (Germuska et al., 2013; Lauwers et al., 2008). As such these  
11 contributions to the qBOLD signal may also provide fertile ground for future exploration.

12

### 13 **Conclusion**

14 The ASE qBOLD signal decay was found to be symmetric with respect to the spin echo, in  
15 contrast to previous simulation of the GESSE pulse sequence. Overestimation of DBV by  
16 ASE based qBOLD was found to be dominated by the effect of diffusion on extravascular  
17 signal decay, with the presence of intravascular blood signal having only a small  
18 contribution. Integrating the results of single vessel simulations using an *in vivo* distribution  
19 of vessel radii revealed several limitations of current measurements and provides a  
20 foundation for future optimisation of ASE based qBOLD acquisitions.

21

### 22 **Acknowledgements**

23 This work was supported by the Engineering and Physical Sciences Research Council [grant  
24 number EP/K025716/1].

25

## 1 **Appendix A**

2 The results of the simulations performed in this study can be accessed via the Oxford  
3 University Research Archive, doi: <https://doi.org/10.5287/bodleian:mvPY99a9D>.  
4 Furthermore, the code used to generate these simulation results and to analyse experimental  
5 data can be downloaded from the Zenodo repository, doi:  
6 <https://doi.org/10.5281/zenodo.2586624>. Supplementary data related to this article can be  
7 found at [<DOI>](#).

8

## 9 **References**

- 10 An, H., Lin, W., 2003. Impact of intravascular signal on quantitative measures of cerebral  
11 oxygen extraction and blood volume under normo- and hypercapnic conditions using an  
12 asymmetric spin echo approach. *Magn. Reson. Med.* 50, 708–716.
- 13 An, H., Lin, W., 2000. Quantitative measurements of cerebral blood oxygen saturation using  
14 magnetic resonance imaging. *J. Cereb. Blood Flow Metab.* 20, 1225–1236.
- 15 Astrup, J., Siesjö, B.K., Symon, L., 1981. Thresholds in cerebral ischemia - the ischemic  
16 penumbra. *Stroke* 12, 723–725.
- 17 Berman, A.J.L., Mazerolle, E.L., MacDonald, M.E., Blockley, N.P., Luh, W.M., Pike, G.B.,  
18 2017. Gas-free calibrated fMRI with a correction for vessel-size sensitivity. *Neuroimage*  
19 169, 176–188.
- 20 Berman, A.J.L., Pike, G.B., 2018. Transverse signal decay under the weak field  
21 approximation: Theory and validation. *Magn. Reson. Med.* 32, 710–749.
- 22 Blockley, N.P., Griffeth, V.E.M., Germuska, M.A., Bulte, D.P., Buxton, R.B., 2013. An  
23 analysis of the use of hyperoxia for measuring venous cerebral blood volume:  
24 Comparison of the existing method with a new analysis approach. *Neuroimage* 72, 33–  
25 40.
- 26 Blockley, N.P., Jiang, L., Gardener, A.G., Ludman, C.N., Francis, S.T., Gowland, P.A., 2008.  
27 Field strength dependence of R1 and R2\* relaxivities of human whole blood to  
28 proance, vasovist, and deoxyhemoglobin. *Magn. Reson. Med.* 60, 1313–1320.
- 29 Boas, D.A., Jones, S.R., Devor, A., Huppert, T.J., Dale, A.M., 2008. A vascular anatomical  
30 network model of the spatio-temporal response to brain activation. *Neuroimage* 40,  
31 1116–1129.
- 32 Bouvier, J., Castellani, S., Debacker, C., Pannetier, N., Troprès, I., Krainik, A., Barbier, E.L.,  
33 2013. Evaluation of multiparametric qBOLD in white matter: a simulation study, in:  
34 *Proc. Intl. Soc. Mag. Reson. Med.* . p. 1.
- 35 Boxerman, J.L., Bandettini, P.A., Kwong, K.K., Baker, J.R., Davis, T.L., Rosen, B.R.,  
36 Weisskoff, R.M., 1995a. The intravascular contribution to fMRI signal change: Monte  
37 Carlo modeling and diffusion-weighted studies in vivo. *Magn. Reson. Med.* 34, 4–10.
- 38 Boxerman, J.L., Hamberg, L.M., Rosen, B.R., Weisskoff, R.M., 1995b. MR contrast due to  
39 intravascular magnetic susceptibility perturbations. *Magn. Reson. Med.* 34, 555–566.
- 40 Christen, T., Pannetier, N.A., Ni, W.W., Qiu, D., Moseley, M.E., Schuff, N., Zaharchuk, G.,  
41 2014. MR vascular fingerprinting: A new approach to compute cerebral blood volume,



- 1 mean vessel radius, and oxygenation maps in the human brain. *Neuroimage* 89, 262–  
2 270.
- 3 Dickson, J.D., Ash, T.W.J., Williams, G.B., Harding, S.G., Carpenter, T.A., Menon, D.K.,  
4 Ansorge, R.E., 2010. Quantitative BOLD: the effect of diffusion. *J. Magn. Reson.*  
5 *Imaging* 32, 953–961.
- 6 Dickson, J.D., Ash, T.W.J., Williams, G.B., Sukstanskii, A.L., Ansorge, R.E., Yablonskiy,  
7 D.A., 2011. Quantitative phenomenological model of the BOLD contrast mechanism. *J.*  
8 *Magn. Reson.* 212, 17–25.
- 9 Dickson, J.D., Williams, G.B., Harding, S.G., Carpenter, T.A., Ansorge, R.E., 2009. Nulling  
10 the CSF Signal in Quantitative fMRI, in: *Proc. Intl. Soc. Mag. Reson. Med.* 17. p. 1640.
- 11 Germuska, M.A., Meakin, J.A., Bulte, D.P., 2013. The influence of noise on BOLD-mediated  
12 vessel size imaging analysis methods. *J. Cereb. Blood Flow Metab.* 33, 1857–1863.
- 13 Griffeth, V.E.M., Buxton, R.B., 2011. A theoretical framework for estimating cerebral  
14 oxygen metabolism changes using the calibrated-BOLD method: Modeling the effects  
15 of blood volume distribution, hematocrit, oxygen extraction fraction, and tissue signal  
16 properties on the BOLD signal. *Neuroimage* 58, 198–212.
- 17 He, X., Yablonskiy, D.A., 2007. Quantitative BOLD: Mapping of human cerebral  
18 deoxygenated blood volume and oxygen extraction fraction: Default state. *Magn. Reson.*  
19 *Med.* 57, 115–126.
- 20 Kety, S.S., Schmidt, C.F., 1948. The nitrous oxide method for the quantitative determination  
21 of cerebral blood flow in man: Theory, procedure and normal values. *J. Clin. Invest.* 27,  
22 476–483.
- 23 Kiselev, V.G., Posse, S., 1999. Analytical model of susceptibility-induced MR signal  
24 dephasing: effect of diffusion in a microvascular network. *Magn. Reson. Med.* 41, 499–  
25 509.
- 26 Lauwers, F., Cassot, F., Lauwers-Cances, V., Puwanarajah, P., Duvernoy, H., 2008.  
27 Morphometry of the human cerebral cortex microcirculation: General characteristics and  
28 space-related profiles. *Neuroimage* 39, 936–948.
- 29 Lee, H., Englund, E.K., Wehrli, F.W., 2018. Interleaved quantitative BOLD  $\square$ : Combining  
30 extravascular  $R^2 \square$  - and intravascular  $R^2$  -measurements for estimation of  
31 deoxygenated blood volume and hemoglobin oxygen saturation. *Neuroimage* 174, 420–  
32 431. <https://doi.org/10.1016/j.neuroimage.2018.03.043>
- 33 Marchal, G., Rioux, P., Petit-Taboué, M.C., Sette, G., Travère, J.M., Le Poec, C.,  
34 Courtheoux, P., Derlon, J.M., Baron, J.C., 1992. Regional cerebral oxygen consumption,  
35 blood flow, and blood volume in healthy human aging. *Arch. Neurol.* 49, 1013–1020.
- 36 Muller, M.E., 1959. A note on a method for generating points uniformly on  $n$ -dimensional  
37 spheres. *Commun. ACM* 2, 19–20.
- 38 Pannetier, N.A., Sohlin, M., Christen, T., Schad, L., Schuff, N., 2014. Numerical modeling of  
39 susceptibility-related MR signal dephasing with vessel size measurement: phantom  
40 validation at 3T. *Magn. Reson. Med.* 72, 646–658.
- 41 Rempp, K.A., Brix, G., Wenz, F., Becker, C.R., Gückel, F., Lorenz, W.J., 1994.  
42 Quantification of regional cerebral blood flow and volume with dynamic susceptibility  
43 contrast-enhanced MR imaging. *Radiology* 193, 637–641.
- 44 Sharan, M., Jones, M.D., Koehler, R.C., Traystman, R.J., Popel, A.S., 1989. A  
45 compartmental model for oxygen transport in brain microcirculation. *Ann. Biomed.*  
46 *Eng.* 17, 13–38.
- 47 Spees, W.M., Yablonskiy, D.A., Oswood, M.C., Ackerman, J.J., 2001. Water proton MR  
48 properties of human blood at 1.5 Tesla: magnetic susceptibility, T1, T2, T2\*, and non-  
49 Lorentzian signal behavior. *Magn. Reson. Med.* 45, 533–542.
- 50 Stone, A.J., Blockley, N.P., 2017. A streamlined acquisition for mapping baseline brain



- 1 oxygenation using quantitative BOLD. *Neuroimage* 147, 79–88.
- 2 Stone, A.J., Harston, G.W.J., Carone, D., Okell, T.W., Kennedy, J., Blockley, N.P., 2019.
- 3 Prospects for investigating brain oxygenation in acute stroke: Experience with a non-
- 4 contrast quantitative BOLD based approach. *Hum. Brain Mapp.*
- 5 Tsai, A.G., Johnson, P.C., Intaglietta, M., 2003. Oxygen gradients in the microcirculation.
- 6 *Physiol. Rev.* 83, 933–963.
- 7 Wismer, G.L., Buxton, R.B., Rosen, B.R., Fisel, C.R., Oot, R.F., Brady, T.J., Davis, K.R.,
- 8 1988. Susceptibility induced MR line broadening: applications to brain iron mapping. *J.*
- 9 *Comput. Assist. Tomogr.* 12, 259–265.
- 10 Yablonskiy, D.A., Haacke, E.M., 1994. Theory of NMR signal behavior in magnetically
- 11 inhomogeneous tissues: the static dephasing regime. *Magn. Reson. Med.* 32, 749–763.
- 12

## Tables

**Table 1.** Vascular compartment model described by (Sharan et al., 1989). Radius, length and number of vessels were used to calculate the relative volume fractions for each compartment with and without arteriolar vessels.

	Arterioles					Capillary		Venules			
	a1	a2	a3	a4	a5	c	v5	v4	v3	v2	v1
Radius ( $\mu\text{m}$ )	60	30	15	10	5	2.8	7.5	15	22.5	45	90
Length ( $\mu\text{m}$ )	5390	2690	1350	900	450	600	450	900	1350	2690	5390
Number of vessels	1880	$1.5 \times 10^4$	$1.15 \times 10^5$	$3.92 \times 10^5$	$3.01 \times 10^6$	$5.92 \times 10^7$	$3.01 \times 10^6$	$3.92 \times 10^5$	$1.15 \times 10^5$	$1.5 \times 10^4$	1880
Relative vol. frac. (%) (all vessel types)	4.3	4.3	4.1	4.1	4.0	32.6	8.9	9.3	9.2	9.6	9.6
Relative vol. frac. (%) (excluding arterioles)						41.2	11.3	11.7	11.6	12.1	12.1

## Figures

**Fig. 1.** By combining the phases generated by the Monte Carlo simulations different pulse sequences can be simulated. The cumulative sum of the phase accumulated after the  $180^\circ$  refocussing pulse is subtracted from the cumulative sum of the phases accumulated prior to the refocussing pulse. In a standard spin echo pulse sequence (a) the refocussing pulse is placed midway between the  $90^\circ$  excitation pulse and the echo time ( $t_E$ ), which is equal to the spin echo time ( $t_{SE}$ ). The GESSE pulse sequence (b) introduces  $R_2'$ -weighting through the parameter  $\tau$  by altering  $t_E$ , whilst keeping  $t_{SE}$  constant. Note: each value of  $\tau$  is acquired at a different  $t_E$ . The ASE sequence (c) introduces  $R_2'$ -weighting by shifting the refocussing pulse by a time  $\tau/2$  leading to a change in  $t_{SE}$ , although  $t_E$  is kept constant. By convention positive values of  $\tau$  occur when the  $t_E > t_{SE}$  and negative values occur when  $t_E < t_{SE}$ .

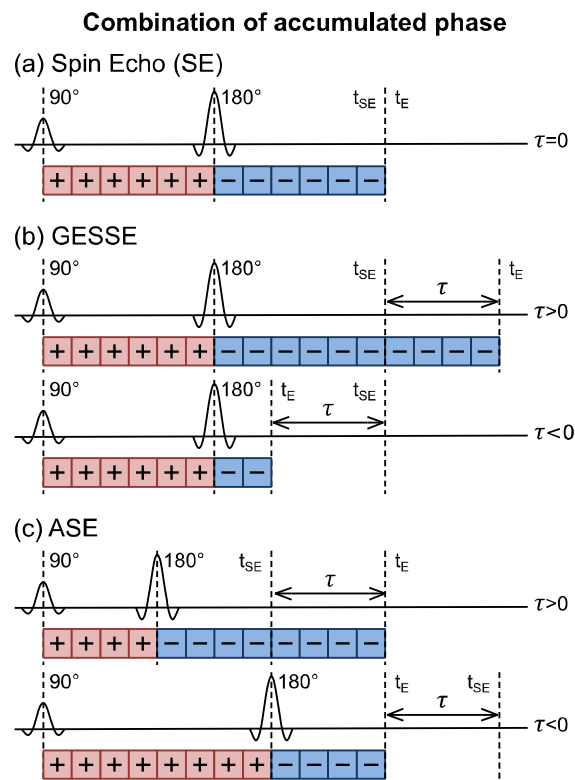


**Fig. 2.** Examples of the signal decay from the ASE pulse sequence as a function of vessel radius. (a) The extravascular signal ( $S_{EV}$ ) decay is observed to be symmetric with respect to  $\tau=0$  regardless of vessel radius. (b) The intravascular signal ( $S_{IV}$ ) decay shows considerable signal attenuation which is symmetric and varies weakly with  $\tau$ .

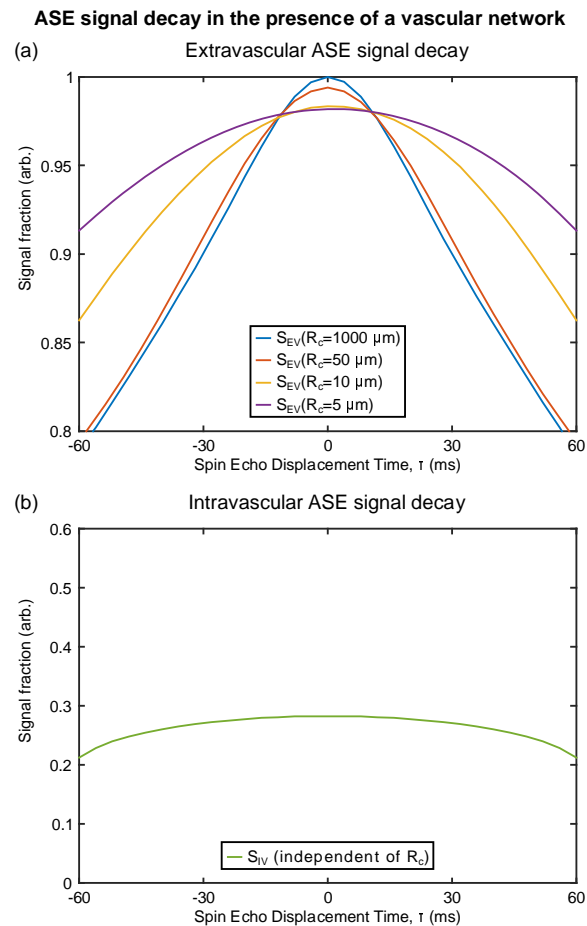


**Fig. 3.** Investigation of the effect of vessel radius on the parameter estimates derived from ASE based qBOLD. Simulations were first performed with a fixed OEF ( $E_0=40\%$ ) and three DBV values (top) then with a fixed DBV ( $V_0=3\%$ ) and three values of OEF (bottom). The apparent  $R_2'$  (left) is estimated for each OEF-DBV pair and presented alongside the  $R_2'$  values predicted by the SDR qBOLD model (dashed lines). Likewise the apparent DBV (centre) and apparent OEF (right) are presented alongside the true DBV and OEF, respectively, (dashed lines).

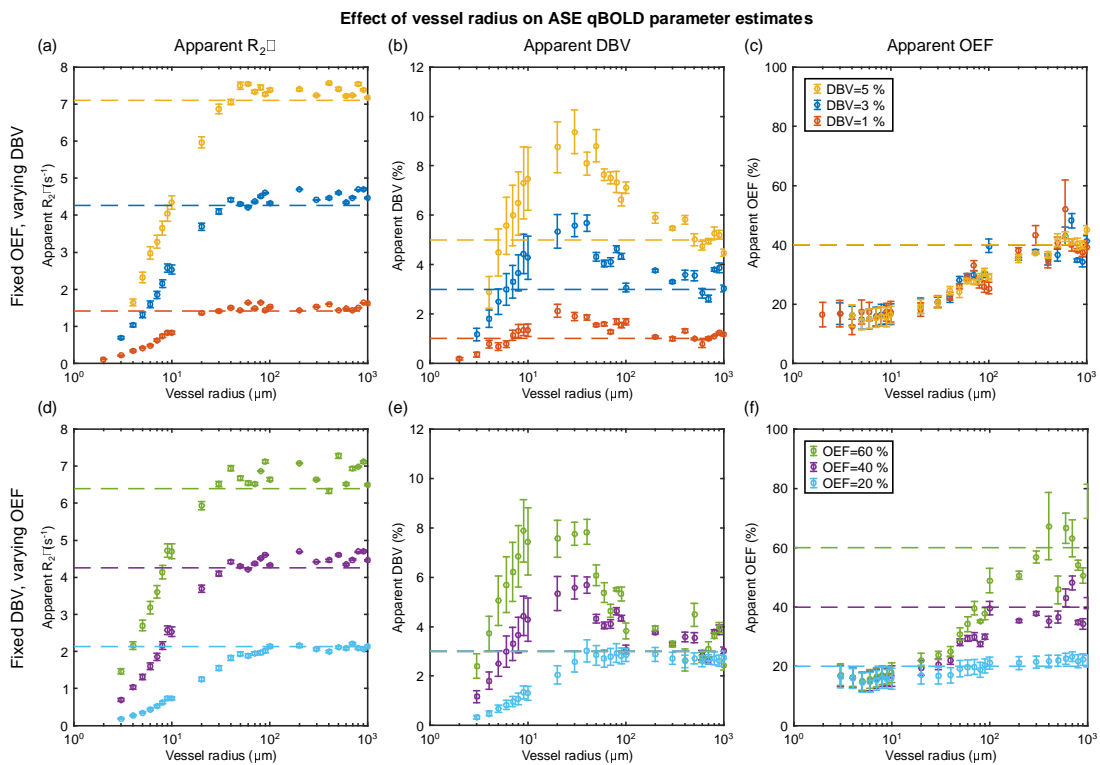


**Fig. 4.** Estimation of the percentage error in DBV at each of the three simulated values with

(a) fixed  $E_0=40\%$ , varying DBV and (b) fixed  $V_0=3\%$ , varying  $E_0$ .

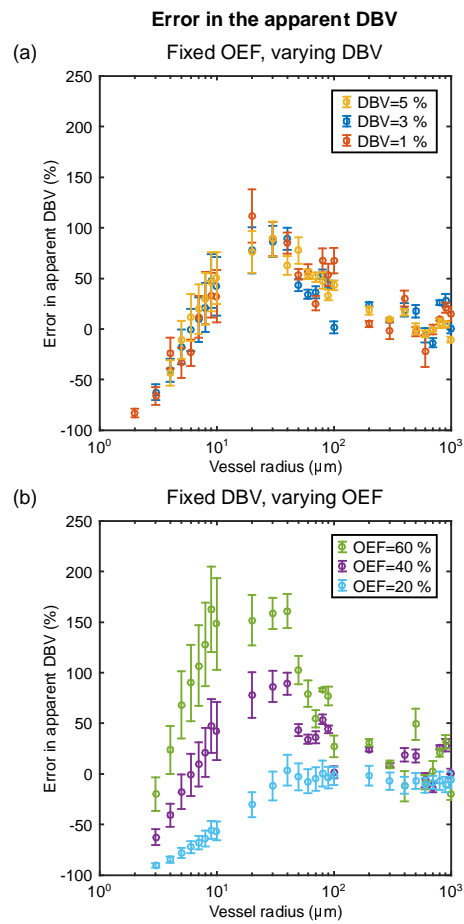


**Fig. 5.** Investigation of the contribution of intravascular signal to qBOLD parameter estimates (PE) presented in Fig. 3. This contribution was quantified as the percentage difference between PEs simulated with and without intravascular signal i.e.  $(PE_{EV} - PE_{EV+IV})/PE_{EV+IV}$ . Extravascular only PE results can be found in supplementary materials (Fig. S5).

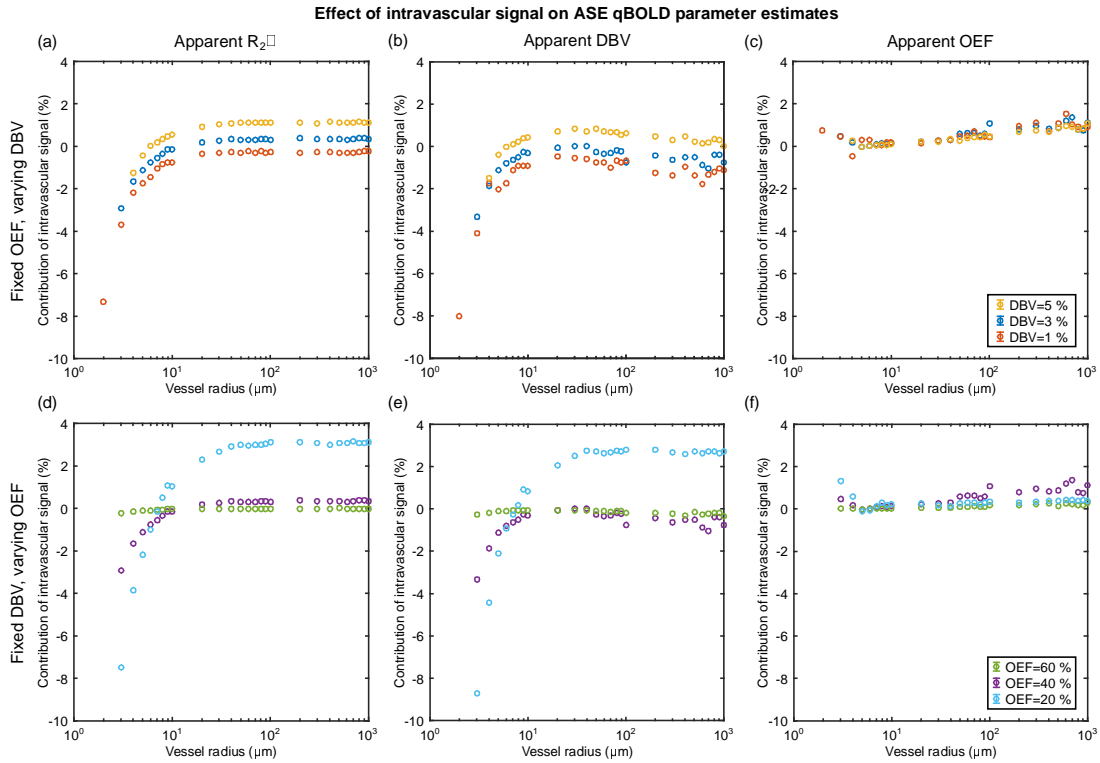


**Fig. 6.** Investigation of the origin of the overestimation of the measured DBV for three different OEF values; (a)  $E_0=60\%$ , (b)  $E_0=40\%$ , (c)  $E_0=20\%$  (true  $V_0=3\%$ ). The orange markers represents natural log of the measured signal at  $\tau=0$ , plotted here as  $-\ln S_{meas}^S(0)$ , whilst the green markers represent the log of the intercept extrapolated from long  $\tau$  data points ( $\ln S_{extrap}^L(0)$ ). The sum of these curves is the apparent DBV as in Fig. 3 and represented here by the grey shaded area. Dashed lines display the prediction made by the SDR qBOLD model.

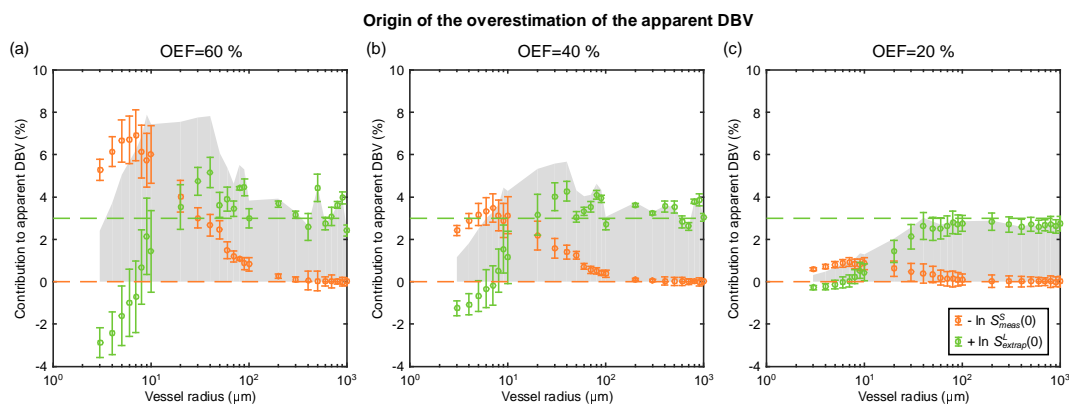




**Fig. 7.** The effect of multiple vessel radii simulations on the qBOLD parameter estimates was considered by generating many pairs of OEF and CBV values. ASE pulse sequence parameters were  $t_E=80$  ms with  $\tau=0$  and  $\tau=16$  to 64 ms in 4 ms steps following the work of (Stone and Blockley, 2017). (a) The apparent  $R_2'$  is linearly dependent on the  $R_2'$  predicted by the SDR model, but with a different gradient. (b) A large amount of uncertainty in the apparent DBV is observed. (c) The apparent OEF appears to plateau beyond 50%, but monotonically increases with true OEF for lower values. Markers are coloured to reflect true dHb content, true OEF and true DBV for parts (a), (b) and (c), respectively.

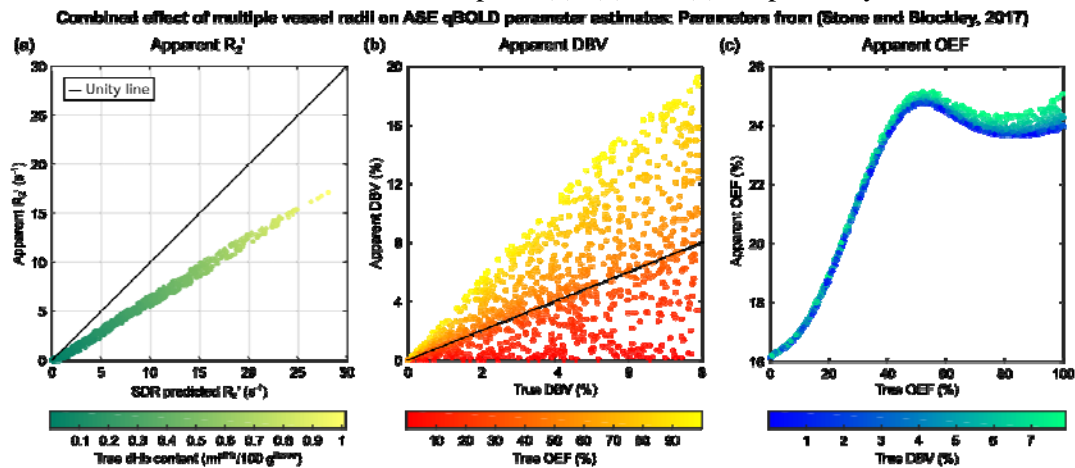


**Fig. 8.** The uncertainty in DBV in Fig. 7 was investigated by plotting apparent DBV as a function of true OEF. ASE pulse sequence parameters follow the work of (Stone and Blockley, 2017). The results suggest that the error in the apparent DBV is OEF dependent. Markers are coloured to reflect their true DBV.

**Multiple vessel radii: Parameters from (Stone and Blockley, 2017)**

